RESEARCH ARTICLE
SPACE PHYSICS: MAGNETOSPHERIC PHYSICS

Earth and Planetary Physics
6: 149–160, 2022
doi: 10.26464/epp2022012

The 600 keV electron injections in the Earth's outer radiation belt: A statistical study

ChaoLing Tang[1*], Xu Wang[2], BinBin Ni[3,4], ZhengPeng Su[5], and JiChun Zhang[6]

[1]Shandong Key Laboratory of Optical Astronomy and Solar-Terrestrial Environment, Institute of Space Sciences, Shandong University, Weihai Shandong 264209, China;

[2]School of Space Science and Physics, Shandong University, Weihai Shandong 264209, China;

[3]Department of Space Physics, School of Electronic Information, Wuhan University, Wuhan 430072, China;

[4]CAS Center for Excellence in Comparative Planetology, Hefei 230026, China;

[5]CAS Key Laboratory of Geospace Environment, Department of Geophysics and Planetary Sciences, University of Science and Technology of China, Hefei 230026, China;

[6]Staunch Data Analytics Lab, Durham, New Hampshire, USA

Key Points:

- Six hundred kiloelectron volt electron injections were observed at $4.5 < L < 6.4$ under different geomagnetic conditions of 450 nT < *AE* < 1,450 nT.
- Before the electron injections, a flux negative *L* shell gradient for ≤0.6 MeV electrons or low electron fluxes in the injected region were observed.
- For 600 keV electron injections at different *L* shells, the source populations from the Earth's plasma sheet were different.

Citation: Tang, C. L., Wang, X., Ni, B. B., Su, Z. P., and Zhang, J. C. (2022). The 600 keV electron injections in the Earth's outer radiation belt: A statistical study. *Earth Planet. Phys.*, *6*(2), 149–160. http://doi.org/10.26464/epp2022012

Abstract: Relativistic electron injections are one of the mechanisms of relativistic (≥0.5 MeV) electron enhancements in the Earth's outer radiation belt. In this study, we present a statistical observation of 600 keV electron injections in the outer radiation belt by using data from the Van Allen Probes. On the basis of the characteristics of different injections, 600 keV electron injections in the outer radiation belt were divided into pulsed electron injections and nonpulsed electron injections. The 600 keV electron injections were observed at $4.5 < L < 6.4$ under the geomagnetic conditions of 450 nT < *AE* < 1,450 nT. An *L* of ~4.5 is an inward limit for 600 keV electron injections. Before the electron injections, a flux negative *L* shell gradient for ≤0.6 MeV electrons or low electron fluxes in the injected region were observed. For 600 keV electron injections at different *L* shells, the source populations from the Earth's plasma sheet were different. For 600 keV electron injections at higher *L* shells, the source populations were higher energy electrons (~200 keV at $X \sim -9\ R_E$), whereas the source populations for 600 keV electron injections at lower *L* shells were lower energy electrons (~80 keV at $X \sim -9\ R_E$). These results are important to further our understanding of electron injections and rapid enhancements of 600 keV electrons in the Earth's outer radiation belt.

Keywords: electron injections; relativistic electrons; the Earth's outer radiation belt; plasma sheet; Van Allen Probes

1. Introduction

The picture of relativistic (≥0.5 MeV) electron acceleration in the Earth's outer radiation belt is a three-step process: substorm electrons (from tens to hundreds of keV) are first injected; then the electrons with energies of hundreds of keV are locally accelerated by whistler mode chorus waves; and subsequently, radial diffusion redistributes the accelerated electrons (e.g., Horne and Thorne, 1998; Meredith et al., 2003; Miyoshi et al., 2003; Reeves et al., 2013; Thorne et al., 2013; Boyd et al., 2014; Mourenas et al., 2014; Omura et al., 2015). Usually, the timescale of the chorus wave acceleration of the electrons with energies of hundreds of keV to megaelectron volt (MeV) energies is greater than ~12 h (e.g., Kasahara et al., 2009; Tsurutani et al., 2010; Miyoshi et al., 2013; Li W et al., 2014; Tang CL et al., 2017a).

However, several other mechanisms can explain the rapid enhancement of relativistic electrons in the Earth's outer radiation belt. The first mechanism is relativistic electron injections. Previous observation and simulation studies have shown that substorm dipolarization electric fields or convection electric fields in the plasma sheet can cause relativistic electron injections at the geosynchronous orbit (e.g., Li X et al., 1998; Kim et al., 2000; Fok et al., 2001; Ingraham et al., 2001; Glocer et al., 2011; Ganushkina et al., 2013; Kress et al., 2014). Multipoint simultaneous observations have also shown that substorm injected electrons in the inner

Correspondence to: C. L. Tang, tcl@sdu.edu.cn
Received 01 SEP 2021; Accepted 27 OCT 2021.
Accepted article online 25 JAN 2022.

magnetosphere can be accelerated to ≥1 MeV (e.g., Su ZP et al., 2014; Dai L et al., 2015; Tang CL et al., 2016b; Kim et al., 2021). The second mechanism is an interplanetary (IP) shock acceleration (e.g., Schiller et al., 2016). The Combined Release and Radiation Effects Satellite (CRRES) first observed prompt acceleration of the electrons in the outer radiation belt by an IP shock compression of the dayside magnetopause during the 24 March 1991 geomagnetic storm (Blake et al., 1992). According to observations by the Van Allen Probes, multi-megaelectron volt (multi-MeV) electron enhancements in the outer radiation belt on less than a drift timescale were caused by the 7 October 2013 and 17 March 2015 IP shock compressions on the dayside (Foster et al., 2014; Baker et al., 2016; Kanekal et al., 2016). Magnetohydrodynamics test particle simulations have also reproduced prompt acceleration of multi-MeV electrons by the 17 March 2015 IP shock (Hudson et al., 2017). The third mechanism may involve the local acceleration of energetic electrons in nonlinear interactions with chorus waves (e.g., Mozer et al., 2014; Tang CL et al., 2016b). Foster et al. (2017) also found that prompt (<1 h) MeV electron acceleration in the inner magnetosphere accompanied substorm injections and strong, very low frequency chorus rising tones. However, relativistic (≥0.5 MeV) electron injections in the Earth's outer radiation belt are still not well understood (e.g., the characteristics of the electron injections and the injection region, as well as the source populations).

In this study, we first present the global distributions of ~600 keV electron injection events in the outer radiation belt from Van Allen Probe observations. We then analyze in detail the two different types of 600 keV electron injection events. Finally, we explain and discuss why 600 keV electron injections can occur at different L shells ($4.5 < L < 6.4$) for different geomagnetic activities (450 nT < AE < 1,450 nT).

2. Observations of 600 keV Electron Injections

To examine 600 keV electron injections in the Earth's outer radiation belt, the Level 2 spin-averaged differential electron flux and the Level 3 pitch angle distributions (PADs) of energetic electrons from a magnetic electron ion spectrometer (MagEIS; Blake et al., 2013) of the Energetic Particle, Composition, and Thermal Plasma Suite (Spence et al., 2013) were used in this study. There were 25 energy channels ranging from 20 to 4,000 keV for electrons from the MagEIS instrument. The criteria for selecting the 600 keV electron injections were as follows:

(1) There were no significant injections within half an hour before injections for the ~600 keV electrons.
(2) For the injected electrons (the cutoff energy was ~600 keV), the maximum flux of electrons was at least 2 times higher than the flux before the electron injections.
(3) Approximately 600 keV electron flux fluctuations during the injections were excluded.

During the time interval from October 2012 to October 2018, 24 events met the selection criteria of 600 keV electron injections. The geomagnetic indices were mainly obtained from the Coordinated Data Analysis Web (http://cdaweb.gsfc.nasa.gov/). The 600 keV electron injection events are listed in Table 1. In Table 1, ε is the upper energy cutoff, J is the peak flux of the 90° pitch angle for ~600 keV electrons, L and MLT represent the locations of 600 keV electron injections, B_z is the z component of the magnetic field in the geocentric solar magnetospheric coordinates observed by the Van Allen Probes. Time refers to the duration of the 600 keV electron injections. In this study, we defined this electron injection event as a "pulsed electron injection event" because of the shorter duration of the 600 keV electron injections (≤4 min), whereas "nonpulsed electron injections" were the 600 keV electron injections of longer duration (>4 min). Types P and NP represented pulsed electron injections and nonpulsed electron injections, respectively. The letter N represents the negative L shell gradients for ≤0.6 MeV electrons in the injected region before the electron injections. For the D injection events, the lower fluxes for ~0.6 MeV electrons before the electron injections were observed and the injection location (L) were less than the location of the flux peak for ~0.6 MeV electrons (L_{peak}) before the electron injections. (The fluxes for ~0.6 MeV electrons before the electron injections in these injection events were less than 100 $cm^{-2}s^{-1}sr^{-1}keV^{-1}$.) Location was where the 600 keV electrons were injected. "Outside" and "inside" indicate that the injection location was outside or inside the plasmasphere, respectively. The L shell of the plasmapause was identified here as a steep density gradient. The AE index was the substorm intensity around the time of the 600 keV electron injections.

Figure 1a shows the global distribution of ~600 keV electron injection events as a function of L and MLT under different geomagnetic conditions. The L value is the calculated McIlwains parameter (with regard to the Earth's radius). Usually, substorm electron injections (up to 100s keV) are observed near the geosynchronous orbit (e.g., Friedel et al., 1996; Reeves et al., 1996; Birn et al., 1998). As shown in Figure 1a, 600 keV electron injection events were mainly located in the dawn sector and at $L > 4.5$. Some dispersive electron injections were also found in the dayside region, and these dayside electron flux enhancements were a result of energetic electron drifting in the inner magnetosphere after dispersionless injection at the nightside. In addition, these 600 keV electron injection events occurred under the geomagnetic conditions of 450 nT < AE < 1,450 nT. Figure 1b shows the flux distribution of ~600 keV electron injections in the L–MLT coordinates. At different L shells, the fluxes for ~600 keV electrons were different.

It is useful to classify the electron injection events according to their injection characteristics. Here we show examples for the two different classifications that were used in the present study. Figure 2 presents the ~600 keV electron injection event observed by Van Allen Probe A between 11:00 and 12:00 UT on 9 December 2014. For this injection event, the onset of the substorm expansion began at 11:19 UT because of the rapid decrease of the AL index (Figure 2b). The AE index reached a maximum of 438 nT at ~11:27 UT (Figure 2a). At ~11:28 UT, a flux increase of 597 keV electrons followed by increases of lower energy electrons (470, 346, 226, 184, 143, and 108 keV) were observed by Van Allen Probe A. This was a typical dispersive injection event (Figure 2c). The duration of 600 keV electron injections was ~1 min, which was a pulsed electron injection event. Because of the azimuthal separation of the injection region and strong background magnetic field, a significant increase in the magnetic field B_z component was not observed by Van Allen Probe A (not shown). For this

Table 1. List of the 600 keV electron injection events examined in this study.

Van Allen Probe	yyyymmdd_ hh–hh	ε (keV)	J ($cm^{-2}s^{-1}$ $sr^{-1}keV^{-1}$)	L	MLT	B_z (nT)	Time (min)	Type (P/NP)	N/D	Location	AE (nT)
A	20121013_17–18	597	27,655	5.97	6.49	120	3	P	N	Outside	1,270
A	20121124_06–07	597	2,125	6.14	5.93	85	4	P	N	Outside	978
A	20130126_09–10	597	1,991	5.70	2.02	142	2	P	N	Outside	775
B	20140209_18–19	597	2,396	5.27	13.5	190	3	P	N	Outside	1,182
A	20141209_11–12	597	2,867	6.11	3.05	92	1	P	N	Outside	447
B	20141209_11–12	597	2,307	6.35	1.96	85	1	P	N	Outside	447
B	20160412_18–19	597	686	6.08	7.37	125	1	P	N	Outside	1,067
A	20180601_10–11	597	4,888	4.82	1.75	228	1	P	D	Outside	1,150
B	20180601_10–11	597	2,434	5.86	3.67	106	1	P	N	Outside	1,150
B	20181001_14–15	597	951	6.15	22.7	145	3	P	N	Outside	881
A	20121014_10–11	597	13,067	5.88	6.39	140	10	NP	N	Outside	951
A	20121014_13–14	597	30,697	5.40	8.14	175	11	NP	N	Outside	1,125
A	20121101_09–10	597	4,380	6.05	6.21	108	11	NP	N	Outside	746
B	20121101_09–10	597	3,357	6.04	6.89	111	11	NP	N	Outside	746
B	20121124_06–07	597	3,560	5.66	4.45	105	6	NP	N	Outside	978
A	20121217_09–10	597	5,081	5.56	3.65	150	6	NP	D	Outside	1,350
A	20140209_18–19	597	2,937	5.64	11.7	164	9	NP	N	Outside	1,280
B	20140209_18–19	597	3,852	5.03	13.8	210	9	NP	N	Outside	1,280
A	20151004_04–05	597	1,824	5.13	13.9	195	5	NP	D	Inside	804
B	20170420_03–04	597	978	4.49	20.1	264	10	NP	D	Inside	1,429
A	20170817_11–12	597	999	4.76	12.0	280	12	NP	D	Inside	1,231
B	20170817_11–12	597	828	4.61	11.1	300	7	NP	D	Inside	1,231
B	20180215_17–18	597	663	5.51	5.11	160	10	NP	D	Outside	618
A	20180826_16–17	597	1,626	6.19	0.06	150	7	NP	N	Outside	1,271

Note. ε = upper energy cutoff; J = peak flux of 90° pitch angle for ~600 keV electrons; L and MLT = locations of 600 keV electron injections; B_z = z component of the magnetic field in the geocentric solar magnetospheric coordinates observed by the Van Allen Probes; Time = duration for 600 keV electron injections; Types (P/NP) = pulsed electron injections and nonpulsed electron injections; N/D = N, negative L shell gradients for ≤0.6 MeV electrons in the injected region before the electron injections, and D, lower fluxes for ~0.6 MeV electrons before the electron injections were observed and the injection location (L) is less than the location of the flux peak for ~0.6 MeV electrons (L_{peak}) before the electron injections; Location = location where 600 keV electrons are injected, where Outside is outside the plasmasphere, and Inside is inside the plasmasphere; AE = substorm intensity around the time of 600 keV electron injections.

injection event, the cutoff energy of injected electrons was 597 keV because the maximum flux of 597 keV electrons at L ~ 6.11 was at least 2 times higher than the flux before the electron injection. For statistical convenience, the "2 times" criterion was used to eliminate the flux increases resulting for various other reasons (e.g., an enhancement of the local magnetic field, satellite movement, and random fluctuations). As shown in Figures 2d–2g, the PADs of injected electrons were ~90° peaked, which is also an electron injection feature. The PAD observations indicated that these electrons experienced betatron acceleration during the injection process (e.g., Northrop, 1963; Tang CL et al., 2013, 2016a, b).

Note that the electron fluxes near the 0° pitch angle in Figure 2 may have been caused by the orientation of that particle detector. Located in the dawn sector (MLT ~ 1.96) and at L ~ 6.35, Van Allen Probe B also observed ~600 keV electron injections after 11:26 UT. In this study, there were 10 pulsed electron injection events, which are labeled P in Table 1.

Figure 3 shows the ~600 keV electron injection event observed by Van Allen Probe B between 16:40 and 17:40 UT on 15 February 2018. For this event, the substorm expansion onset began at ~17:00 UT. The AE index reached a maximum of 618 nT at ~17:13

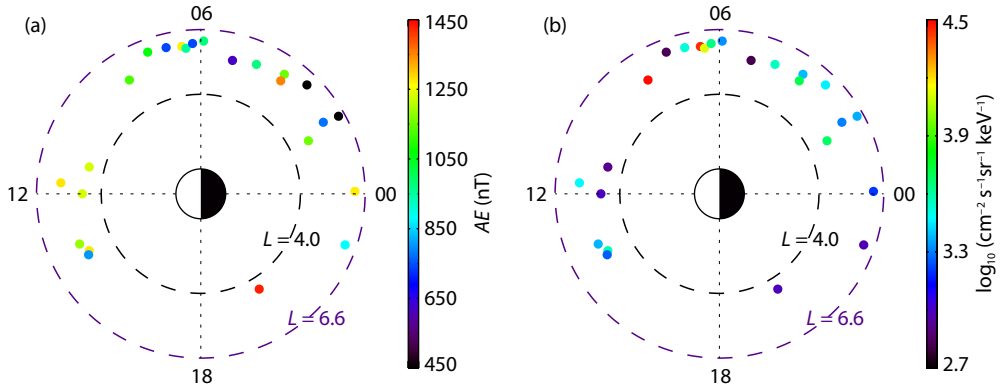

Figure 1. (a) The global distributions of ~600 keV electron injection events as a function of *L* and *MLT* under different geomagnetic conditions. The purple dashed circle shows *L* ~ 6.6, and the black dashed circle shows *L* ~ 4.0. The color bar indicates the substorm intensity for ~600 keV electron injection events. (b) The flux distributions of ~600 keV electron injections as a function of *L* and *MLT*. The color bar indicates the fluxes for ~600 keV electrons.

UT (Figure 3a). At ~17:04 UT, Van Allen Probe B observed a flux increase of 604 keV electrons, followed by increases of lower energy electrons (470, 354, 240, 208, 168, and 132 keV; Figure 3c). The duration of 600 keV electron injections was ~10 min, which were nonpulsed electron injection events. As shown in Figures 3d–3g, the PADs of substorm injected electrons were ~90° peaked. Note that the electron fluxes near the 180° pitch angle in Figure 3 may have been due to the orientation of the particle detector. In this study, there were 14 nonpulsed electron injection events, which are labeled NP in Table 1.

We categorized the injection events into two groups, pulsed electron injections and nonpulsed electron injections, by considering the different injection characteristics of the 600 keV electron injections. Figure 4a shows the substorm intensity versus the *L* shells of the peak fluxes of ~600 keV electrons during 600 keV electron injection events from October 2012 to October 2018. Some pulsed electron injection events were observed at higher *L* shells ($L > 6.0$) during the weaker geomagnetic activities (*AE* ~450 nT). Some nonpulsed electron injections were observed at smaller *L* shells (*L* ~4.5) during the intense geomagnetic activities (*AE* ~1,450 nT). In Figure 4b, the local magnetic fields (dominated by the B_z component) were stronger at smaller *L* shells (*L* ~4.5–5.0), whereas the local magnetic fields were weaker at higher *L* shells (*L* ~6.0). These B_z components during 600 keV electron injections observed by the Van Allen Probes were close to the dipole field at $L < 5.5$ and were lower than the dipole field at $L > 5.5$ (see the black line in Figure 4b).

In Figure 5, we plotted the electron fluxes from each inbound and outbound pass for different E_k (E_k of 102–604 keV) for the 600 keV electron injection event on 9 December 2014. This allowed us to examine how the electron flux profile evolved in time before and during the electron injections. This was a pulsed electron injection event. Before the electron injections, the electron flux peaks were at *L* ~5.0. The fluxes had negative gradients for E_k ~ 200–600 keV electrons at higher *L* shells (*L* ~6.0). During the electron injections (after ~11:27 UT), the fluxes had a similar evolution for different electrons. For E_k ~200–600 keV electrons, there were sudden, pulsed increases in fluxes near the apogee of the Van Allen Probes ($L > 6.1$) (Figures 5c–5f), which came from the plasma sheet and may have been accompanied by a dipolarization front (DF) or magnetic pulse. This injection was also seen by the LANL-97A satellite (not shown). Before the 600 keV electron injections, the injection regions for some injection events also had negative *L* shell gradients. For this injection event, the *L* shell of the plasmapause was ~4.5; thus, the injection location was outside the plasmasphere (see Table 1).

Figure 6 shows the electron fluxes at different E_k (E_k of 103–584 keV) measured by the Van Allen Probes (A and B) as a function of *L* during the time interval from 01:42 to 14:33 UT on 17 August 2017. This was a nonpulsed electron injection event. Before the electron injections, the flux peaks for E_k ~200–600 keV electrons were at higher *L* shells (*L* ~ 6.0; Figures 6c–6f). The fluxes for E_k ~200–600 keV electrons at *L* ~4.5 were smaller, which indicated that the Earth's outer radiation belt is in a state of depletion. At ~11:50 UT, there were large, sudden increases in the fluxes for 300–600 keV electrons at *L* ~4.5–4.8 (Figures 6d–6f). This event was followed by enhancement over a wide range of *L* ($L > 4.8$), which may have been due to the acceleration of radial diffusion (Figures 6d–6f). For the low-energy electrons (100–200 keV), there were strong enhancements at *L* ~ 3.5–5.8 during and after the electron injections (Figures 6a–6c). These features were likely associated with a substorm injection and were identified by the peak in *AE* at 12:00 UT. Before the 600 keV electron injections, low electron fluxes were also observed in the injection region for some events. For this injection event, the *L* shell of the plasmapause was approximately 5.0; thus, the injection location was inside the plasmasphere (see Table 1).

Figures 7a–7g presents the ~600 keV electron injection event observed by Van Allen Probe A between 10:00 and 11:00 UT on 1 June 2018. The *AE* index reached a maximum of 1,150 nT at ~10:13 UT (Figure 7a). At ~10:18 UT, Van Allen Probe A observed a flux increase of 597 keV electrons followed by increases of lower energy electrons (470, 340, 226, 184, 143, and 108 keV; Figure 2c). The duration of 600 keV electron injections was less than 1 min, which was also a pulsed electron injection event. As shown in Figures 7d–7g, the PADs of injected electrons were ~90° peaked.

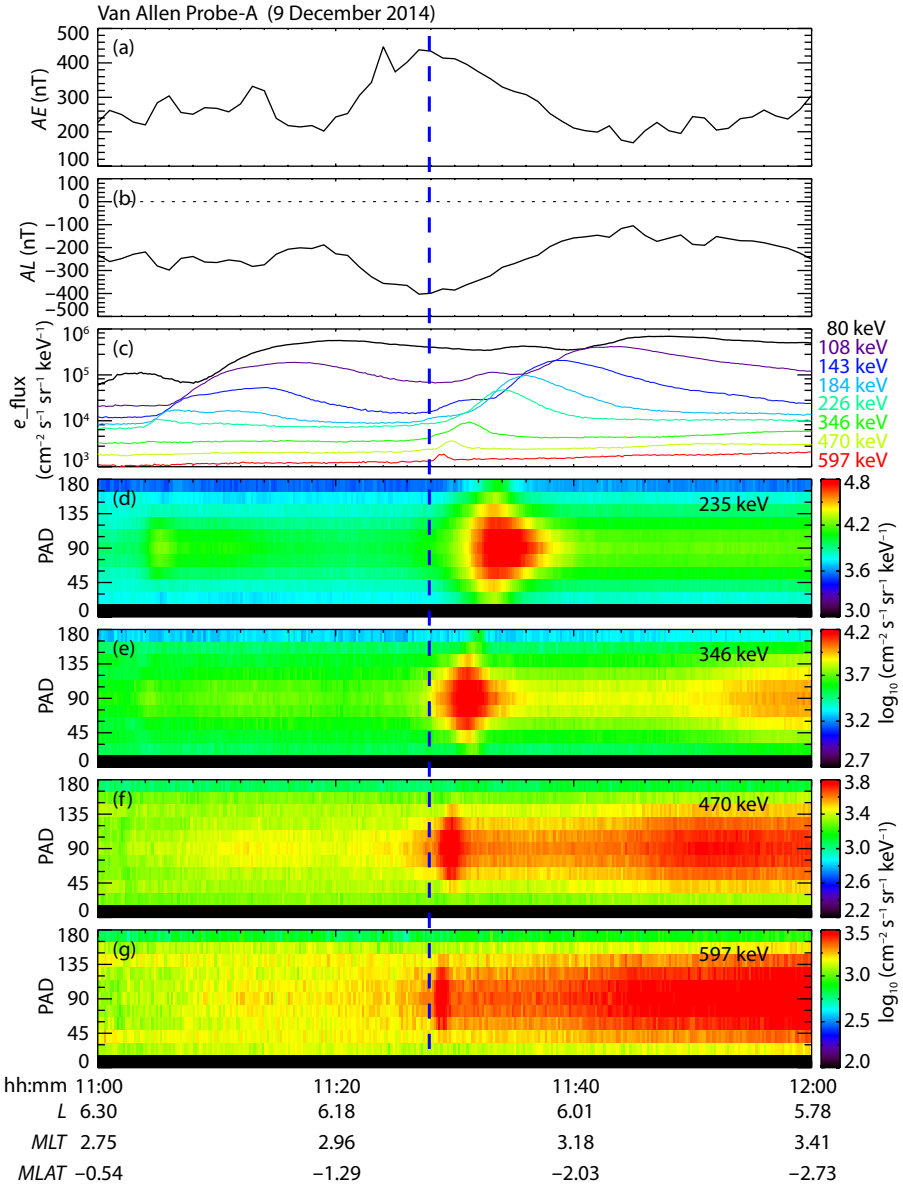

Figure 2. The ~600 keV electron injection event on 9 December 2014 observed by Van Allen Probe A. From top to bottom for each column: the geomagnetic indices (*AE* and *AL*), the differential fluxes of energetic electrons, and the PADs of different electrons (235–597 keV) from the MagEIS instrument. The vertical blue dashed line shows the time of electron injections.

Figures 7h–7n shows the total magnetic field B_t, the magnetic field ***B*** observed by the Fluxgate magnetometer, the fluxes of energetic electrons observed by the solid-state telescope (SST), and the electron PADs in the SST energy range during the time interval from 10:14 to 10:16 UT on 1 June 2018, observed by P5. P5 was located at −5.3, 10.7, and 1.5 R_E in the geocentric solar magnetospheric coordinates. The B_x component at P5 was approximately −20 nT (Figure 7i), which indicates that P5 was away from the neutral sheet. At ~10:14:45 UT (indicated by the vertical blue dashed line in Figure 7, left), the B_z component began to increase, whereas the B_z component was up to the peak at ~10:14:48 UT, which is a characteristic signal of a DF. At the DF, P5 observed enhanced energetic electron fluxes and quasi-perpendicular distributions (near 90°; Figures 7j–7n). Using the simultaneous observations of the near-Earth magnetotail and outer radiation belt, we provided evidence that the energetic electrons (~120 keV) associated with the DF observed by P5 (Figure 7m) could be the source population of the injected 600 keV electrons at *L* ~4.8 observed by Van Allen Probe A (Figure 7g). Assume that enhanced 600 keV electrons in the outer radiation belt during the substorm recovery phase observed by Van Allen Probe A came from the DF at the near-Earth tail (at P5). In the outer radiation belt, the magnetic field strength B_t was up to 232 nT. The magnetic field strength B_{t0} in the near-Earth tail was ~44 nT, and then B_t/B_{t0} was approximately 5.3. When the formula of the first adiabatic invariant was used, the initial energy of the electrons in the near-Earth tail was ~120 keV, and the accelerated energy of the electrons at *L* ~4.8 could be up to ~600 keV. Observations also showed that the fluxes of 120 keV electrons in the near-Earth tail (at P5) were larger than the increased fluxes of ~600 keV electrons at Van Allen

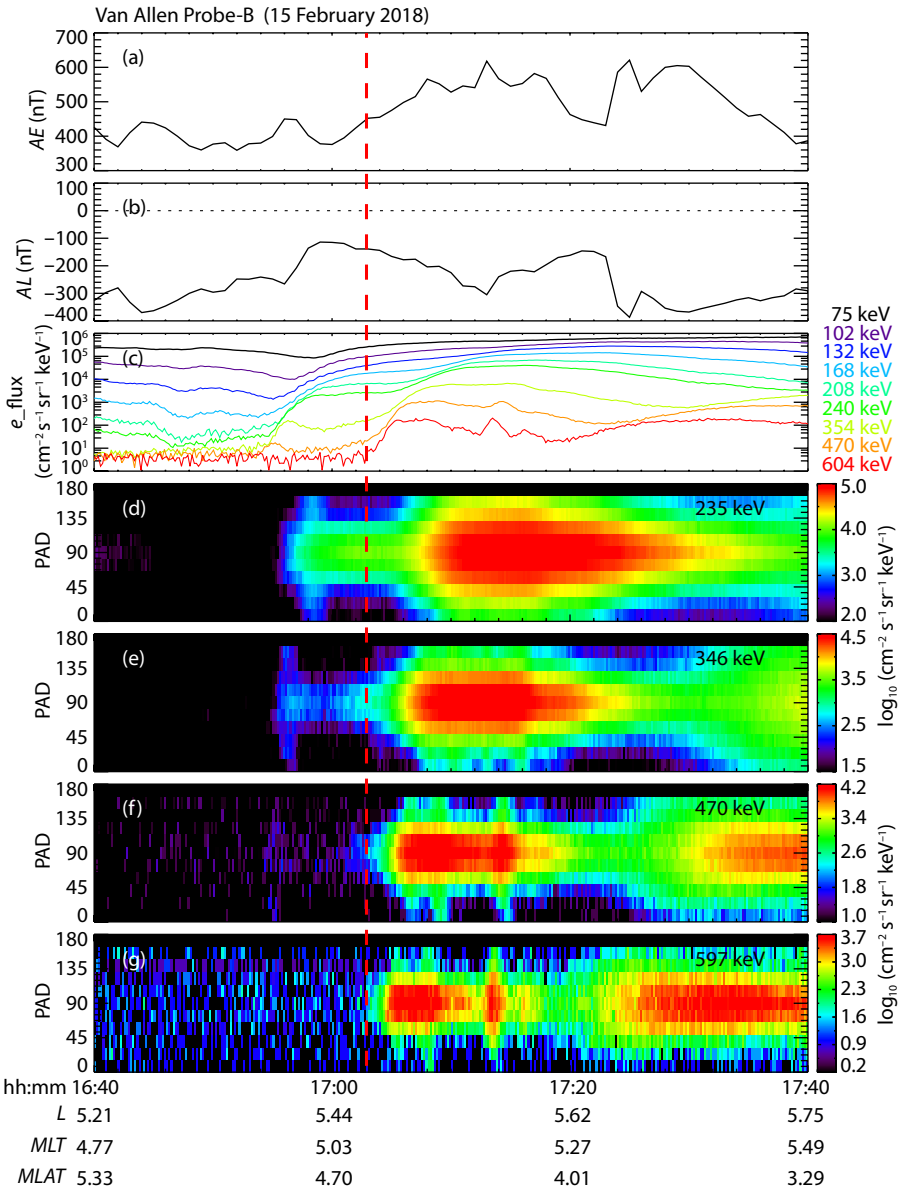

Figure 3. The ~600 keV electron injection event on 15 February 2018 observed by Van Allen Probe B. From top to bottom for each column: the geomagnetic indices (*AE* and *AL*), the differential fluxes of energetic electrons, and the PADs of different electrons (235–597 keV) from the MagEIS instrument. The vertical red dashed line shows the time of electron injections.

Probe A (Figure 3c). These showed that betatron acceleration was the main acceleration mechanism during the injection process of ~600 keV electrons.

3. Discussion and Summary

Substorm injections are sudden enhancements of the particles with energies from tens to hundreds of keV (e.g., Moore et al., 1981; Reeves et al., 1990; Duan et al., 2021), which are usually associated with a magnetic field dipolarization. Generally, the dipolarization includes two forms: substorm dipolarization and a DF (e.g., Tang CL et al., 2013). Substorm dipolarization, with a duration of up to tens of minutes, propagates tailward and is associated with the earthward transport of particles during the substorm expansion phase (e.g., Lui ATY, 1991; Ohtani et al., 1992; Baker et al., 1996; Nakamura et al., 2009; Tang CL et al., 2009, 2017b, 2018). The DFs or magnetic pulses have a duration of tens of seconds or a short time (≲4 min) and propagate toward the Earth (e.g., Nakamura et al., 2002; Runov et al., 2009; Tang CL et al., 2010, 2016a, 2021). In general, electron injections in the Earth's outer radiation belt are associated with DFs (e.g., Dai L et al., 2015; Turner et al., 2015, 2016; Motoba et al., 2020). Using the data from Van Allen Probes, Liu J et al. (2016) showed that energetic particle injections in the cis-geosynchronous magnetosphere ($L < 6.6$) are associated with dipolarizing flux bundles. These electron injections accompanied by DFs can contribute to rapid enhancements of relativistic electrons in the outer radiation belt (e.g., Dai L et al., 2015). However, Fok et al. (2001) and Ingraham et al. (2001) showed that substorm dipolarization can cause relativistic electron injections at the geosynchronous orbit. Tang CL et al. (2016b) also showed that prompt enhancements of MeV electrons in the

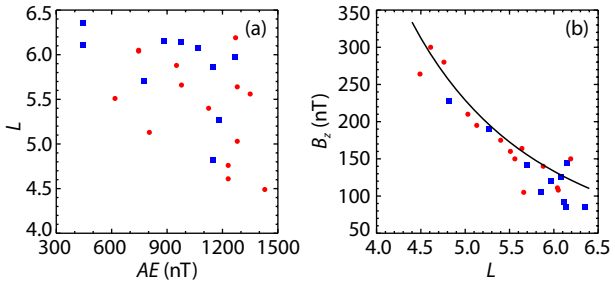

Figure 4. (a) Substorm intensity (*AE*) versus the *L* shells of the peak fluxes of ~600 keV electrons during 600 keV electron injection events from October 2012 to October 2018; (b) The *L* shells versus the B_z components during 600 keV electron injections observed by the Van Allen Probes. In the figure, the blue squares denote pulsed electron injection events, and the red dots denote nonpulsed electron injection events, respectively. In (b), the black line shows the magnetic field (the B_z component) from the dipole model.

outer radiation belt are associated with substorm dipolarization. In this study, pulsed electron injection events may be associated with DFs or magnetic pulses, and nonpulsed electron injection events may be associated with substorm dipolarizations in the Earth's plasma sheet.

Intense electric fields are one of the principal factors affecting relativistic electron injections in the outer radiation belt. Previous studies have shown that these intense substorm electric fields or enhanced transient electric fields can accelerate injected electrons in the outer radiation belt (e.g., Mithaiwala and Horton, 2005; Gabrielse et al., 2012; Dai L et al., 2014, 2015; Tang CL et al., 2016b). Furthermore, other factors (e.g., the characteristics of the injection region before electron injections and the source populations) may affect ~600 keV electron injections in the outer radiation belt.

Previous studies have shown that electron energy and the plasmapause location can affect the injected depth of the electrons. Because of the effects of the gradient and curvature drifting for >500 keV electrons, the convection cannot inject them far inward (e.g., Reeves et al., 1996; Liu S et al., 2003). The energetic particle injections inside the geosynchronous orbit are limited to $L > 4$ (e.g., Friedel et al., 1996; Sergeev et al., 1998). Turner et al. (2015) showed that electron injections at $L \leqslant 4$ are limited in energy to ⩽250 keV. In this study, *L* ~4.5 was an inward limit for 600 keV electron injections. These 600 keV electron injections at lower *L* shells may filter out higher energy electrons that are injected at higher *L* shells because of the effects of the gradient and curvature drifts. In general, the plasmapause location shrinks as the geomagnetic activity increases. Khoo et al. (2019) showed that the initial enhancements of energetic electrons (~30 to ~2.5 MeV) are typically outside the innermost plasmapause locations regardless of the solar wind drivers and the geomagnetic activity. However, some observations have shown that substorm hot electrons can be injected into the plasmasphere (e.g., Thorne et al., 1979; Meredith et al., 2004; Chen L et al., 2014; Su ZP et al., 2018). In this study, these injected events could appear either outside or inside the plasmasphere (see Table 1). This may be related to the flux negative *L* shell gradient of ≤0.6 MeV electrons (Figure 5) or the low electron fluxes in the injected region before the electron injections (Figure 6) and the source populations of ~600 keV injected electrons.

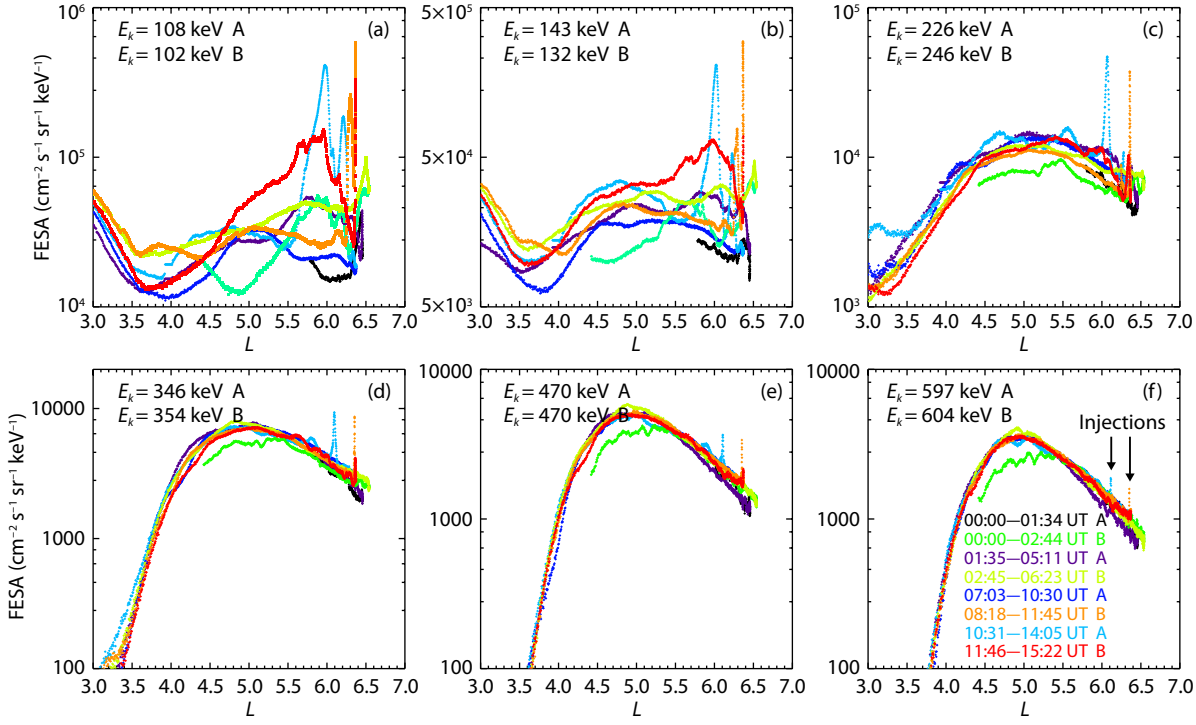

Figure 5. Electron fluxes at different E_k (E_k of 102–604 keV) measured by the Van Allen Probes (A and B) as a function of *L* during the time interval from 00:00 to 15:22 UT on 9 December 2014.

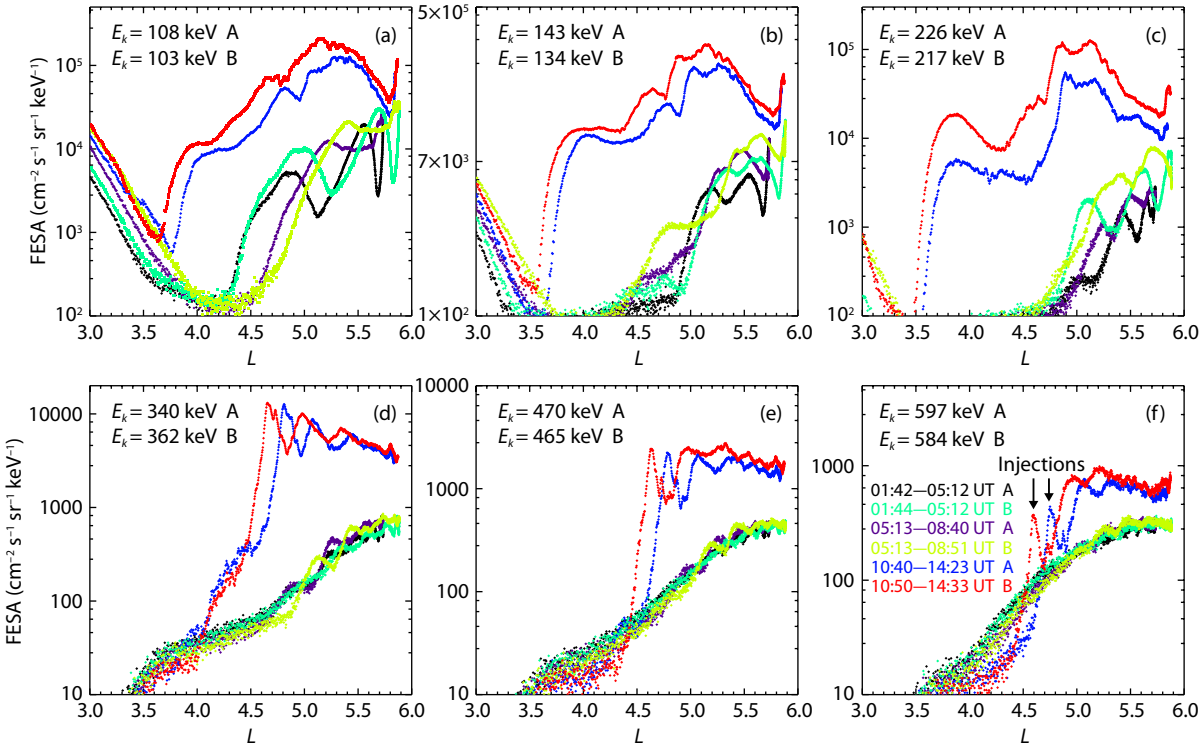

Figure 6. Electron fluxes at different E_k (E_k of 103–597 keV) measured by the Van Allen Probes (A and B) as a function of L during the time interval from 01:42 to 14:33 UT on 17 August 2017.

Previous observations have shown that energetic electrons in the mid-tail or the near-Earth magnetotail during geomagnetic activities are the source population of injected MeV electrons in the outer radiation belt (e.g., Taylor et al., 2004; Lui ATY et al., 2012; Dai L et al., 2014; Tang CL et al., 2016b). During the injection of energetic electrons, these electrons move earthward and enter the region of a stronger magnetic field (mainly the B_z component, as shown by Tverskoy, 1969). These electrons mainly conserved the first adiabatic invariant (see Figures 2d–2g and 3d–3g). Although these accelerated electrons originated from different initial locations in the plasma sheet, we assumed that the source locations of ~600 keV electron injections were in the near-Earth plasma sheet (at X ~ –9 R_E) to compare the initial electron energy for 600 keV electron injections at different L shells (4.5 < L < 6.4). Previous studies have shown that the magnetic field (the B_z component) associated with a substorm dipolarization or DF in the near-Earth plasma sheet (at X ~ –9 R_E) was about 30 nT during the betatron acceleration process (e.g., Tang CL et al., 2009; Runov et al., 2011; Liu J et al., 2013; Tang CL et al., 2016b, 2021). Using the formula of the first adiabatic invariant, we were able to show that these accelerated electrons (~600 keV) at different L shells may have different source populations from the plasma sheet. For 24 injection events, the upper energy cutoff (ε_{max}) was ~600 keV, and the magnetic field (B_{zi}) in the near-Earth plasma sheet (at X ~ –9 R_E) was assumed to be 30 nT. Considering relativistic effects, the energy (ε_i) at X ~ –9 R_E for 600 keV electrons in the injections at L ~ 6.0 was about 200 keV, whereas the energy (ε_i) at X ~ –9 R_E for 600 keV electrons in the injections at L ~ 4.5 was ~80 keV. Note that these electron populations at X ~ –9 R_E may be accompanied by different magnetic structures (DFs, magnetic pulses, or substorm dipolarizations). The present study suggests that betatron acceleration may be the main acceleration mechanism for ~600 keV electrons during the injection processes. However, previous studies have shown that whistler-mode waves occur at DFs and during substorm dipolarizations (e.g., Le Cont et al., 2009; Zhou M et al., 2009; Deng XH et al., 2010; Khotyaintsev et al., 2011; Huang SY et al., 2012; Fu HS., et al., 2014). These waves may contribute to nonadiabatic acceleration during the injection processes, although they are not discussed in detail here. These results suggest that the energy of the source population was higher for ~600 keV electron injections at higher L shells, whereas the energy of the source population was smaller for ~600 keV electron injections at lower L shells.

On the basis of the preceding analysis and discussion, we explain why 600 keV electron injections were observed at 4.5 < L < 6.4 under different geomagnetic conditions of 450 nT < AE < 1,450 nT. For 600 keV electron injections at higher L shells (the flux negative L shell gradient for ⩽0.6 MeV electrons in the injected region), the source population for 600 keV electrons was higher energy electrons (~200 keV at X ~ –9 R_E). These electrons could be transported into higher L shells under the electric and magnetic fields. For 600 keV electron injections at lower L shells (the low electron fluxes in the injected region), the source population for 600 keV electrons was lower energy electrons (~80 keV at X ~ –9 R_E). These electrons were less affected by the gradient and curvature drifts and could be injected into lower L shells.

In this study, we present the statistical observation of 600 keV electron injections in the Earth's outer radiation belt. The main conclusions are summarized as follows:

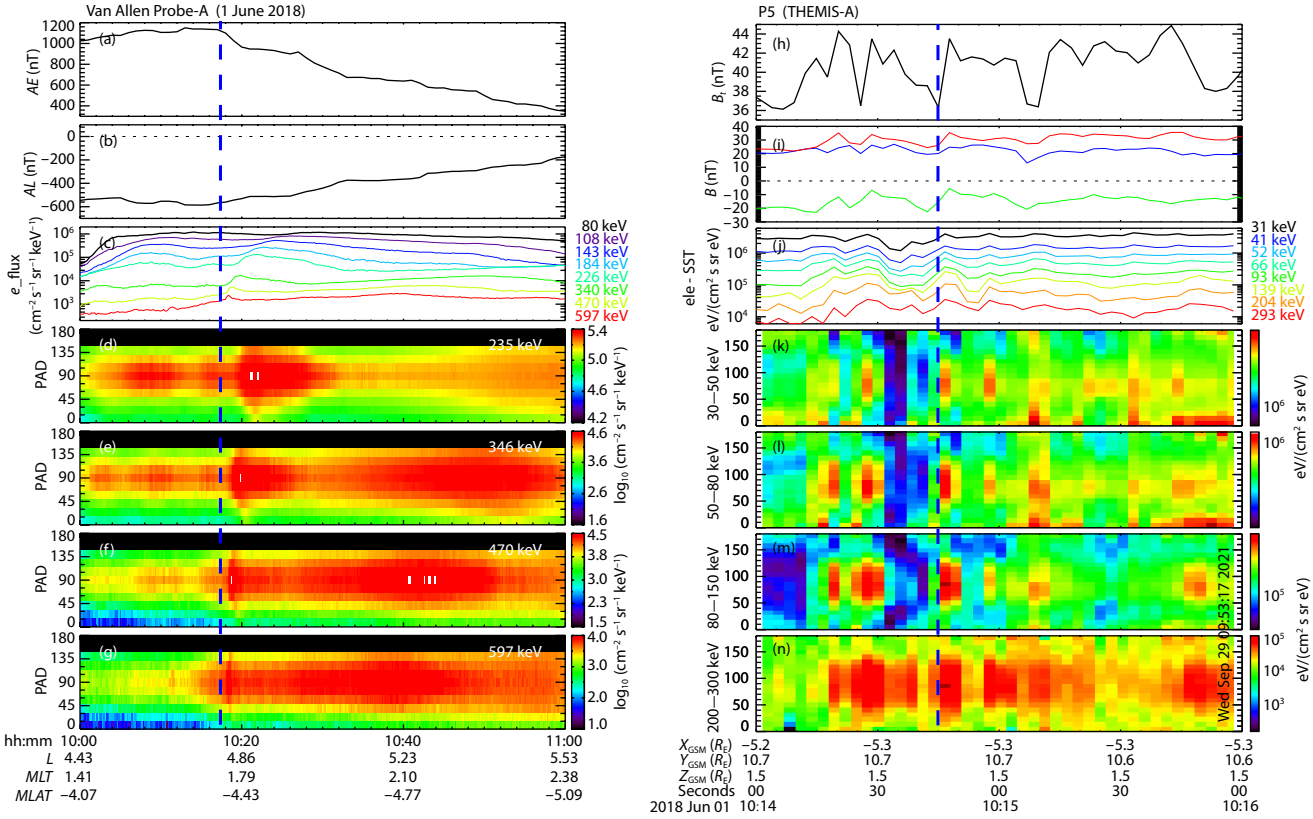

Figure 7. (a–g) The ~600 keV electron injection event on 1 June 2018 observed by Van Allen Probe A, showing the geomagnetic indices (*AE* and *AL*), the differential fluxes of energetic electrons, and the PADs of different electrons (235–597 keV) from the MagEIS instrument. The vertical blue dashed line shows the time of electron injections. (h–n) The THEMIS-A observations during the time interval of 10:14–10:16 UT on 1 June 2018, showing the total magnetic field B_t, the magnetic field $\boldsymbol{B}$ by the Fluxgate magnetometer, the fluxes of energetic electrons observed by the SST, and the electron PADs in the SST energy range (30–300 keV). The vertical blue dashed line indicates the time of the onset of the positive B_z variation. All vectors are in geocentric solar magnetospheric coordinates.

(1) The 600 keV electron injections in the outer radiation belt were divided into pulsed electron injections and nonpulsed electron injection events.

(2) The 600 keV electron injections were mostly observed at $4.5 < L < 6.4$ under the geomagnetic conditions of 450 nT < *AE* < 1,450 nT. An *L* of ~4.5 is an inward limit for 600 keV electron injections.

(3) Before the electron injections, a flux negative *L* shell gradient for ≤0.6 MeV electrons or low electron fluxes in the injected region were observed.

(4) For 600 keV electron injections at different *L* shells, the source populations from the Earth's plasma sheet were different.

Acknowledgments

Van Allen Probe data are available from the following website: https://www.rbsp-ect.lanl.gov/data_pub/. We thank V. Angelopoulos for the use of data from the THEMIS mission. THEMIS data are available at http://themis.ssl.berkeley.edu/data/themis/. We acknowledge the Coordinated Data Analysis Web (http://cdaweb.gsfc.nasa.gov/) for the use of geomagnetic indices. This work was supported by the National Natural Science Foundation of China under grant 41974188.

References

Baker, D. N., Pulkkinen, T. I., Angelopoulos, V., Baumjohann, W., and McPherron, R. L. (1996). Neutral line model of substorms: Past results and present view. *J. Geophys. Res.*: *Space Phys.*, *101*(A6), 12975–13010. https://doi.org/10.1029/95JA03753

Baker, D. N., Jaynes, A. N., Kanekal, S. G., Foster, J. C., Erickson, P. J., Fennell, J. F., Blake, J. B., Zhao, H., Li, X., … Wygant, J. R. (2016). Highly relativistic radiation belt electron acceleration, transport, and loss: Large solar storm events of March and June 2015. *J. Geophys. Res.*: *Space Phys.*, *121*(7), 6647–6660. https://doi.org/10.1002/2016JA022502

Birn, J., Thomsen, M. F., Borovsky, J. E., Reeves, G. D., McComas, D. J., Belian, R. D., and Hesse, M. (1998). Substorm electron injections: Geosynchronous observations and test particle simulations. *J. Geophys. Res.*, *103*(A5), 9235–9248. https://doi.org/10.1029/97JA02635

Blake, J. B., Kolasinski, W. A., Fillius, R. W., and Mullen, E. G. (1992). Injection of electrons and protons with energies of tens of MeV into *L* < 3 on 24 March 1991. *Geophys. Res. Lett.*, *19*(8), 821–824. https://doi.org/10.1029/92GL00624

Blake, J. B., Carranza, P. A., Claudepierre, S. G., Clemmons, J. H., Crain, W. R., Dotan, Y., Fennell, J. F., Fuentes, F. H., Galvan, R. M., … Zakrzewski, M. P. (2013). The *Magnetic Electron Ion Spectrometer* (MagEIS) instruments aboard the Radiation Belt Storm Probes (RBSP) spacecraft. *Space Sci. Rev.*, *179*(1-4), 383–421. https://doi.org/10.1007/s11214-013-9991-8

Boyd, A. J., Spence, H. E., Claudepierre, S. G., Fennell, J. F., Blake, J. B., Baker, D. N., Reeves, G. D., and Turner, D. L. (2014). Quantifying the radiation belt seed population in the 17 March 2013 electron acceleration event. *Geophys. Res. Lett.*, *41*(7), 2275–2281. https://doi.org/10.1002/2014GL059626

Chen, L. J., Thorne, R. M., Bortnik, J., Li, W., Horne, R. B., Reeves, G. D., Kletzing, C. A., Kurth, W. S., Hospodarsky, G. B., … Fennell, J. F. (2014). Generation of

unusually low frequency plasmaspheric hiss. *Geophys. Res. Lett.*, *41*(16), 5702–5709. https://doi.org/10.1002/2014GL060628

Dai, L., Wygant, J. R., Cattell, C. A., Thaller, S., Kersten, K., Breneman, A., Tang, X. W., Friedel, R. H., Claudepierre, S. G., and Tao, X. (2014). Evidence for injection of relativistic electrons into the Earth's outer radiation belt via intense substorm electric fields. *Geophys. Res. Lett.*, *41*(4), 1133–1141. https://doi.org/10.1002/2014GL059228

Dai, L., Wang, C., Duan, S. P., He, Z. H., Wygant, J. R., Cattell, C. A., Tao, X., Su, Z. P., Kletzing, C., … Tang, X. W. (2015). Near-Earth injection of MeV electrons associated with intense dipolarization electric fields: Van Allen Probes observations. *Geophys. Res. Lett.*, *42*(15), 6170–6179. https://doi.org/10.1002/2015GL064955

Deng, X. H., Ashour-Abdalla, M., Zhou, M., Walker, R., El-Alaoui, M., Angelopoulos, V., Ergun R. E., and Schriver, D. (2010). Wave and particle characteristics of earthward electron injections associated with dipolarization fronts. *J. Geophys. Res.*: *Space Phys.*, *115*(A9), A09225. https://doi.org/10.1029/2009JA015107

Duan, S. P., Wang, C., Liu, W. W. and He, Z. H. (2021). Characteristics of magnetic dipolarizations in the vicinity of the substorm onset region observed by THEMIS. *Earth Planet. Phys.*, *5*(3), 239–250. https://doi.org/10.26464/epp2021031

Fok, M. C., Moore, T. E., and Spjeldvik, W. N. (2001). Rapid enhancement of radiation belt electron fluxes due to substorm dipolarization of the geomagnetic field. *J. Geophys. Res.*: *Space Phys.*, *106*(A3), 3873–3881. https://doi.org/10.1029/2000JA000150

Foster, J. C., Erickson, P. J., Baker, D. N., Claudepierre, S. G., Kletzing, C. A., Kurth, W., Reeves, G. D., Thaller, S. A., Spence, H. E., … Wygant, J. R. (2014). Prompt energization of relativistic and highly relativistic electrons during a substorm interval: Van Allen Probes observations. *Geophys. Res. Lett.*, *41*(1), 20–25. https://doi.org/10.1002/2013GL058438

Foster, J. C., Erickson, P. J., Omura, Y., Baker, D. N., Kletzing, C. A., and Claudepierre, S. G. (2017). Van Allen Probes observations of prompt MeV radiation belt electron acceleration in nonlinear interactions with VLF chorus. *J. Geophys. Res.*: *Space Phys.*, *122*(1), 324–339. https://doi.org/10.1002/2016JA023429

Friedel, R. H. W., Korth, A., and Kremser, G. (1996). Substorm onsets observed by CRRES: Determination of energetic particle source regions. *J. Geophys. Res.*: *Space Phys.*, *101*(A6), 13137–13154. https://doi.org/10.1029/96ja00399

Fu, H. S., Cao, J. B., Cully, C. M., Khotyaintsev, Y. V., Vaivads, A., Angelopoulos, V., Zong, Q. G., Santolík, O., Macúšová, E., … Zhima, M. (2014). Whistler-mode waves inside flux pileup region: Structured or unstructured. *J. Geophys. Res.*: *Space Phys.*, *119*(11), 9089–9100. https://doi.org/10.1002/2014JA020204

Gabrielse, C., Angelopoulos, V., Runov, A., and Turner, D. L. (2012). The effects of transient, localized electric fields on equatorial electron acceleration and transport toward the inner magnetosphere. *J. Geophys. Res.*: *Space Phys.*, *117*(A10), A10213. https://doi.org/10.1029/2012JA017873

Ganushkina, N. Y., Amariutei, O. A., Shprits, Y. Y., and Liemohn, M. W. (2013). Transport of the plasma sheet electrons to the geostationary distances. *J. Geophys. Res.*: *Space Phys.*, *118*(1), 82–98. https://doi.org/10.1029/2012JA017923

Glocer, A., Fok, M. C., Nagai, T., Tóth, G., Guild, T., and Blake, J. (2011). Rapid rebuilding of the outer radiation belt. *J. Geophys. Res.*: *Space Phys.*, *116*(A9), A09213. https://doi.org/10.1029/2011JA016516

Horne, R. B., and Thorne, R. M. (1998). Potential waves for relativistic electron scattering and stochastic acceleration during magnetic storms. *Geophys. Res. Lett.*, *25*(15), 3011–3014. https://doi.org/10.1029/98GL01002

Huang, S. Y., Zhou, M., Deng, X. H., Yuan, Z. G., Pang, Y., Wei, Q., Su, W., Li, H. M., and Wang, Q. Q. (2012). Kinetic structure and wave properties associated with sharp dipolarization front observed by Cluster. *Ann. Geophys.*, *30*(1), 97–107. https://doi.org/10.5194/angeo-30-97-2012

Hudson, M., Jaynes, A., Kress, B., Li, Z., Patel, M., Shen, X. C., Thaller, S., Wiltberger, M., and Wygant, J. (2017). Simulated prompt acceleration of multi-MeV electrons by the 17 March 2015 interplanetary shock. *J. Geophys. Res.*: *Space Phys.*, *122*(10), 10036–10046. https://doi.org/10.1002/2017JA024445

Ingraham, J. C., Cayton, T. E., Belian, R. D., Christensen, R. A., Friedel, R. H. W., Meier, M. M., Reeves, G. D., and Tuszewski, M. (2001). Substorm injection of relativistic electrons to geosynchronous orbit during the great magnetic storm of March 24, 1991. *J. Geophys. Res.*: *Space Phys.*, *106*(A11), 25759–25776. https://doi.org/10.1029/2000JA000458

Kanekal, S. G., Baker, D. N., Fennell, J. F., Jones, A., Schiller, Q., Richardson, I. G., Li, X., Turner, D. L., Califf, S., … Wygant, J. R. (2016). Prompt acceleration of magnetospheric electrons to ultrarelativistic energies by the 17 March 2015 interplanetary shock. *J. Geophys. Res.*: *Space Phys.*, *121*(8), 7622–7635. https://doi.org/10.1002/2016JA022596

Kasahara, Y., Miyoshi, Y., Omura, Y., Verkhoglyadova, O. P., Nagano, I., Kimura, I., and Tsurutani, B. T. (2009). Simultaneous satellite observations of VLF chorus, hot and relativistic electrons in a magnetic storm "recovery" phase. *Geophys. Res. Lett.*, *36*(1), L01106. https://doi.org/10.1029/2008GL036454

Khoo, L. Y., Li, X., Zhao, H., Chu, X., Xiang, Z., and Zhang, K. (2019). How sudden, intense energetic electron enhancements correlate with the innermost plasmapause locations under various solar wind drivers and geomagnetic conditions. *J. Geophys. Res.*: *Space Phys.*, *124*(11), 8992–9002. https://doi.org/10.1029/2019JA027412

Khotyaintsev, Y. V., Cully, C. M., Vaivads, A., André, M., and Owen, C. J. (2011). Plasma jet braking: Energy dissipation and nonadiabatic electrons. *Phys. Rev. Lett.*, *106*(16), 165001. https://doi.org/10.1103/PhysRevLett.106.165001

Kim, H. J., Chan, A. A., Wolf, R. A., and Birn, J. (2000). Can substorms produce relativistic outer belt electrons. *J. Geophys. Res.*: *Space Phys.*, *105*(A4), 7721–7735. https://doi.org/10.1029/1999JA900465

Kim, H. J., Lee, D. Y., Wolf, R., Bortnik, J., Kim, K. C., Lyons, L., Choe, W., Noh, S. J., Choi, K. E., … Li, J. (2021). Rapid injections of MeV electrons and extremely fast step-like outer radiation belt enhancements. *Geophys. Res. Lett.*, *48*(9), e2021GL093151. https://doi.org/10.1029/2021GL093151

Kress, B. T., Hudson, M. K., and Paral, J. (2014). Rebuilding of the Earth's outer electron belt during 8–10 October 2012. *Geophys. Res. Lett.*, *41*(3), 749–754. https://doi.org/10.1002/2013GL058588

Le Contel, O., Roux, A., Jacquey, C., Robert, P., Berthomier, M., Chust, T., Grison, B., Angelopoulos, V., Sibeck, D., … Singer, H. (2009). Quasi-parallel whistler mode waves observed by THEMIS during near-Earth dipolarizations. *Ann. Geophys.*, *27*(6), 2259–2275. https://doi.org/10.5194/angeo-27-2259-2009

Li, W., Thorne, R. M., Ma, Q., Ni, B., Bortnik, J., Baker, D. N., Spence, H. E., Reeves, G. D., Kanekal, S. G., … Claudepierre, S. G. (2014). Radiation belt electron acceleration by chorus waves during the 17 March 2013 storm. *J. Geophys. Res.*: *Space Phys.*, *119*(6), 4681–4693. https://doi.org/10.1002/2014JA019945

Li, X., Baker, D. N., Temerin, M., Reeves, G. D., and Belian, R. D. (1998). Simulation of dispersionless injections and drift echoes of energetic electrons associated with substorms. *Geophys. Res. Lett.*, *25*(20), 3763–3766. https://doi.org/10.1029/1998GL900001

Liu, J., Angelopoulos, V., Runov, A., and Zhou, X. Z. (2013). On the current sheets surrounding dipolarizing flux bundles in the magnetotail: The case for wedgelets. *J. Geophys. Res.*: *Space Phys.*, *118*(5), 2000–2020. https://doi.org/10.1002/jgra.50092

Liu, J., Angelopoulos, V., Zhang, X. J., Turner, D. L., Gabrielse, C., Runov, A., Li, J. X., Funsten, H. O., and Spence, H. E. (2016). Dipolarizing flux bundles in the cis-geosynchronous magnetosphere: Relationship between electric fields and energetic particle injections. *J. Geophys. Res.*: *Space Phys.*, *121*(2), 1362–1376. https://doi.org/10.1002/2015JA021691

Liu, S., Chen, M. W., Lyons, L. R., Korth, H., Albert, J. M., Roeder, J. L., Anderson, P. C., and Thomsen, M. F. (2003). Contribution of convective transport to stormtime ring current electron injection. *J. Geophys. Res.*: *Space Phys.*, *107*(A10), 1372. https://doi.org/10.1029/2003JA010004

Lui, A. T. Y. (1991). A synthesis of magnetospheric substorm models. *J. Geophys. Res.*: *Space Phys.*, *96*(A2), 1849–1856. https://doi.org/10.1029/90JA02430

Lui, A. T. Y., Zong, Q. G., Wang, C., and Dunlop, M. W. (2012). Electron source associated with dipolarization at the outer boundary of the radiation belts: Non-storm cases. *J. Geophys. Res.*: *Space Phys.*, *117*(A10), A10224. https://doi.org/10.1029/2012JA018084

Meredith, N. P., Cain, M., Horne, R. B., Thorne, R. M., Summers, D., and Anderson, R. R. (2003). Evidence for chorus-driven electron acceleration to relativistic

energies from a survey of geomagnetically disturbed periods. *J. Geophys. Res.*: *Space Phys.*, *108*(A6), 1248. https://doi.org/10.1029/2002JA009764

Meredith, N. P., Horne, R. B., Thorne, R. M., Summers, D., and Anderson, R. R. (2004). Substorm dependence of plasmaspheric hiss. *J. Geophys. Res.*: *Space Phys.*, *109*(A6), A06209. https://doi.org/10.1029/2004JA010387

Mithaiwala, M. J., and Horton, W. (2005). Substorm injections produce sufficient electron energization to account for MeV flux enhancements following some storms. *J. Geophys. Res.*: *Space Phys.*, *110*(A7), A07224. https://doi.org/10.1029/2004JA010511

Miyoshi, Y., Morioka, A., Misawa, H., Obara, T., Nagai, T., and Kasahara, Y. (2003). Rebuilding process of the outer radiation belt during the 3 November 1993 magnetic storm: NOAA and Exos-D observations. *J. Geophys. Res.*: *Space Phys.*, *108*(A1), 1004. https://doi.org/10.1029/2001JA007542

Miyoshi, Y., Kataoka, R., Kasahara, Y., Kumamoto, A., Nagai, T., and Thomsen, M. F. (2013). High-speed solar wind with southward interplanetary magnetic field causes relativistic electron flux enhancement of the outer radiation belt via enhanced condition of whistler waves. *Geophys. Res. Lett.*, *40*(17), 4520–4525. https://doi.org/10.1002/grl.50916

Moore, T. E., Arnoldy, R. L., Feynman, J., and Hardy, D. A. (1981). Propagating substorm injection fronts. *J. Geophys. Res.*: *Space Phys.*, *86*(A8), 6713–6726. https://doi.org/10.1029/JA086iA08p06713

Motoba, T., Ohtani, S., Claudepierre, S. G., Reeves, G. D., Ukhorskiy, A. Y., and Lanzerotti, L. J. (2020). Dynamic properties of particle injections inside geosynchronous orbit: A multisatellite case study. *J. Geophys. Res.*: *Space Phys.*, *125*(9), e2020JA028215. https://doi.org/10.1029/2020JA028215

Mourenas, D., Artemyev, A. V., Agapitov, O. V., and Krasnoselskikh, V. (2014). Consequences of geomagnetic activity on energization and loss of radiation belt electrons by oblique chorus waves. *J. Geophys. Res.*: *Space Phys.*, *119*(4), 2775–2796. https://doi.org/10.1002/2013JA019674

Mozer, F. S., Agapitov, O., Krasnoselskikh, V., Lejosne, S., Reeves, G. D., and Roth, I. (2014). Direct observation of radiation belt electron acceleration from electron volt energies to megavolts by non-linear whistlers. *Phys. Rev. Lett.*, *113*, 035001. https://doi.org/10.1103/PhysRevLett.113.035001

Nakamura, R., Baumjohann, W., Klecker, B., Bogdanova, Y., Balogh, A., Rème, H., Bosqued, J. M., Dandouras, I., Sauvaud, J. A., … Runov, A. (2002). Motion of the dipolarization front during a flow burst event observed by Cluster. *Geophys. Res. Lett.*, *29*(20), 1942. https://doi.org/10.1029/2002GL015763

Nakamura, R., Retinò, A., Baumjohann, W., Volwerk, M., Erkaev, N., Klecker, B., Lucek, E. A., Dandouras, I., André, M., and Khotyaintsev, Y. (2009). Evolution of dipolarization in the near-Earth current sheet induced by earthward rapid flux transport. *Ann. Geophys.*, *27*(4), 1743–1754. https://doi.org/10.5194/angeo-27-1743-2009

Northrop, T. G. (1963). Adiabatic charged-particle motion. *Rev. Geophys.*, *1*(3), 283–304. https://doi.org/10.1029/RG001i003p00283

Ohtani, S., Takahashi, K., Zanetti, L. J., Potemra, T. A., McEntire, R. W., and Iijima, T. (1992). Initial signatures of magnetic field and energetic particle fluxes at tail reconfiguration: Explosive growth phase. *J. Geophys. Res.*: *Space Phys.*, *97*(A12), 19311–19324. https://doi.org/10.1029/92JA01832

Omura, Y., Miyashita, Y., Yoshikawa, M., Summers, D., Hikishima, M., Ebihara, Y., and Kubota, Y. (2015). Formation process of relativistic electron flux through interaction with chorus emissions in the Earth's inner magnetosphere. *J. Geophys. Res.*: *Space Phys.*, *120*(11), 9545–9562. https://doi.org/10.1002/2015JA021563

Reeves, G. D., Fritz, T. A., Cayton, T. E., and Belian, R. D. (1990). Multi-satellite measurements of the substorm injection region. *Geophys. Res. Lett.*, *17*(11), 2015–2018. https://doi.org/10.1029/GL017i011p02015

Reeves, G. D., Henderson, M. G., McLachlan, P. S., Belian, R. D., Friedel, R. H. W., and Korth, A. (1996). Radial propagation of substorm injections. In E. J. Rolfe et al. (Eds.), *Proceedings of the 3rd International Conference on Substorms* (pp. 579–584). Versailles, France: European Space Agency.

Reeves, G. D., Spence, H. E., Henderson, M. G., Morley, S. K., Friedel, R. H. W., Funsten, H. O., Baker, D. N., Kanekal, S. G., Blake, J. B., … Niehof, J. T. (2013). Electron acceleration in the heart of the Van Allen radiation belts. *Science*, *341*(6149), 991–994. https://doi.org/10.1126/science.1237743

Runov, A., Angelopoulos, V., Sitnov, M. I., Sergeev, V. A., Bonnell, J., McFadden, J. P., Larson, D., Glassmeier, K. H., and Auster, U. (2009). THEMIS observations of an earthward-propagating dipolarization front. *Geophys. Res. Lett.*, *36*(14), L14106. https://doi.org/10.1029/2009GL038980

Runov, A., Angelopoulos, V., Zhou, X. Z., Zhang, X. J., Li, S., Plaschke, F., and Bonnell, J. (2011). A THEMIS multicase study of dipolarization fronts in the magnetotail plasma sheet. *J. Geophys. Res.*: *Space Phys.*, *116*(A5), A05216. https://doi.org/10.1029/2010JA016316

Schiller, Q., Kanekal, S. G., Jian, L. K., Li, X., Jones, A., Baker, D. N., Jaynes, A., and Spence, H. E. (2016). Prompt injections of highly relativistic electrons induced by interplanetary shocks: A statistical study of Van Allen Probes observations. *Geophys. Res. Lett.*, *43*(24), 12317–12324. https://doi.org/10.1002/2016GL071628

Sergeev, V. A., Shukhtina, M. A., Rasinkangas, R., Korth, A., Reeves, G. D., Singer, H. J., Thomsen, M. F., and Vagina, L. I. (1998). Event study of deep energetic particle injections during substorm. *J. Geophys. Res.*, *103*(A5), 9217–9234. https://doi.org/10.1029/97JA03686

Spence, H. E., Reeves, G. D., Baker, D. N., Blake, J. B., Bolton, M., Bourdarie, S., Chan, A. A., Claudepierre, S. G., Clemmons, J. H., … Thorne, R. M. (2013). Science goals and overview of the Radiation Belt Storm Probes (RBSP) energetic particle, composition, and thermal plasma (ECT) suite on NASA's Van Allen probes mission. *Space Sci. Rev.*, *179*(1-4), 311–336. https://doi.org/10.1007/s11214-013-0007-5

Su, Z. P., Zhu, H., Xiao, F. L., Zheng, H. N., Wang, Y. M., Zong, Q. G., He, Z. G., Shen, C., Zhang, M., … Baker, D. N. (2014). Quantifying the relative contributions of substorm injections and chorus waves to the rapid outward extension of electron radiation belt. *J. Geophys. Res.*: *Space Phys.*, *119*(12), 10023–10040. https://doi.org/10.1002/2014JA020709

Su, Z. P., Liu, N. G., Zheng, H. N., Wang, Y. M., and Wang, S. (2018). Multipoint observations of nightside plasmaspheric hiss generated by substorm-injected electrons. *Geophys. Res. Lett.*, *45*(20), 10921–10932. https://doi.org/10.1029/2018GL079927

Tang, C. L., Li, Z. Y., Angelopoulos, V., Mende, S. B., Glassmeier, K. H., Donovan, E., Russell, C. T., and Lu, L. (2009). THEMIS observations of the near-Earth plasma sheet during a substorm. *J. Geophys. Res.*: *Space Phys.*, *114*(A9), A09211. https://doi.org/10.1029/2008JA013729

Tang, C. L., Angelopoulos, V., Runov, A., Russell, C. T., Frey, H., Glassmeier, K. H., Fornacon, K. H., and Li, Z. Y. (2010). Precursor activation and substorm expansion associated with observations of a dipolarization front by Time History of Events and Macroscale Interactions during Substorms (THEMIS). *J. Geophys. Res.*, *115*(A7), A07215. https://doi.org/10.1029/2009JA014879

Tang, C. L., Lu, L., Zhou, M., and Yao, Z. H. (2013). THEMIS observations of electron acceleration associated with the evolution of substorm dipolarization in the near-Earth tail. *J. Geophys. Res.*: *Space Phys.*, *118*(7), 4237–4247. https://doi.org/10.1002/jgra.50418

Tang, C. L., Zhou, M., Yao, Z. H., and Shi, F. (2016a). Electron acceleration associated with the magnetic flux pileup regions in the near-Earth plasma sheet: A multicase study. *J. Geophys. Res.*: *Space Phys.*, *121*(5), 4331–4342. https://doi.org/10.1002/2016JA022406

Tang, C. L., Zhang, J. C., Reeves, G. D., Su, Z. P., Baker, D. N., Spence, H. E., Funsten, H. O., Blake, J. B., and Wygant, J. R. (2016b). Prompt enhancement of the Earth's outer radiation belt due to substorm electron injections. *J. Geophys. Res.*: *Space Phys.*, *121*(12), 11826–11838. https://doi.org/10.1002/2016JA023550

Tang, C. L., Wang, Y. X., Ni, B., Su, Z. P., Reeves, G. D., Zhang, J. C., Baker, D. N., Spence, H. E., Funsten, H. O., and Blake, J. B. (2017a). The effects of magnetospheric processes on relativistic electron dynamics in the Earth's outer radiation belt. *J. Geophys. Res.*: *Space Phys.*, *122*(10), 9952–9968. https://doi.org/10.1002/2017JA024407

Tang, C. L., Wang, Y. X., Ni, B., Zhang, J. C., Reeves, G. D., Su, Z. P., Baker, D. N., Spence, H. E., Funsten, H. O., and Blake, J. B. (2017b). Radiation belt seed population and its association with the relativistic electron dynamics: A statistical study. *J. Geophys. Res.*: *Space Phys.*, *122*(5), 5261–5276. https://doi.org/10.1002/2017JA023905

Tang, C. L., Xie, X. J., Ni, B., Su, Z. P., Reeves, G. D., Zhang, J. C., Baker, D. N., Spence, H. E., Funsten, H. O., … Dai, G Y. (2018). Rapid enhancements of the seed populations in the heart of the Earth's outer radiation belt: A multicase study. *J. Geophys. Res.*: *Space Phys.*, *123*(6), 4895–4907.

https://doi.org/10.1029/2017JA025142

Tang, C. L., Wang, X., and Zhou, M. (2021). Electron pitch angle distributions around dipolarization fronts at the off magnetic equator. *J. Geophys. Res.: Space Phys.*, *126*(2), e2020JA028787. https://doi.org/10.1029/2020JA028787

Taylor, M. G. G. T., Friedel, R. H. W., Reeves, G. D., Dunlop, M. W., Fritz, T. A., Daly, P. W., and Balogh, A. (2004). Multisatellite measurements of electron phase space density gradients in the Earth's inner and outer magnetosphere. *J. Geophys. Res.: Space Phys.*, *109*(A5), A05220. https://doi.org/10.1029/2003JA010294

Thorne, R. M., Church, S. R., and Gorney, D. J. (1979). On the origin of plasmaspheric hiss: The importance of wave propagation and the plasmapause. *J. Geophys. Res.: Space Phys.*, *84*(A9), 5241–5247. https://doi.org/10.1029/JA084iA09p05241

Thorne, R. M., Li, W., Ni, B., Ma, Q., Bortnik, J., Chen, L., Baker, D. N., Spence, H. E., Reeves, G. D., … Kanekal, S. G. (2013). Rapid local acceleration of relativistic radiation-belt electrons by magnetospheric chorus. *Nature*, *504*(7480), 411–414. https://doi.org/10.1038/nature12889

Tsurutani, B. T., Horne, R. B., Pickett, J. S., Santolik, O., Schriver, D., and Verkhoglyadova, O. P. (2010). Introduction to the special section on Chorus: Chorus and its role in space weather. *J. Geophys. Res.: Space Phys.*, *115*(A9), A00F01. https://doi.org/10.1029/2010JA015870

Turner, D. L., Claudepierre, S. G., Fennell, J. F., O'Brien, T. P., Blake, J. B., Lemon, C., Gkioulidou, M., Takahashi, K., Reeves, G. D., … Angelopoulos, V. (2015). Energetic electron injections deep into the inner magnetosphere associated with substorm activity. *Geophys. Res. Lett.*, *42*(7), 2079–2087. https://doi.org/10.1002/2015GL063225

Turner, D. L., Fennell, J. F., Blake, J. B., Clemmons, J. H., Mauk, B. H., Cohen, I. J., Jaynes, A. N., Craft, J. V., Wilder, F. D., … Burch, J. L. (2016). Energy limits of electron acceleration in the plasma sheet during substorms: A case study with the Magnetospheric Multiscale (MMS) mission. *Geophys. Res. Lett.*, *43*(15), 7785–7794. https://doi.org/10.1002/2016GL069691

Tverskoy, B. A. (1969). Main mechanisms in the formation of the Earth's radiation belts. *Rev. Geophys.*, *7*(1-2), 219–231. https://doi.org/10.1029/RG007i001p00219

Zhou, M., Ashour-Abdalla, M., Deng, X. H., Schriver, D., El-Alaoui, M., and Pang, Y. (2009). THEMIS observation of multiple dipolarization fronts and associated wave characteristics in the near-Earth magnetotail. *Geophys. Res. Lett.*, *36*(20), L20107. https://doi.org/10.1029/2009GL040663